Nanoscale Horizons

ROYAL SOCIETY OF CHEMISTRY

COMMUNICATION

View Article Online
View Journal | View Issue

Cite this: *Nanoscale Horiz.*, 2024, 9, 472

Received 18th September 2023,
Accepted 9th January 2024

DOI: 10.1039/d3nh00409k

rsc.li/nanoscale-horizons

Surfactant-tail control of $CsPbBr_3$ nanocrystal morphology†

Yoarhy A. Amador-Sánchez,[a] Brenda Vargas,[b] Josué E. Romero-Ibarra,[c] Rubén Mendoza-Cruz,[c] Estrella Ramos[c] and Diego Solis-Ibarra*[a]

$CsPbBr_3$ nanocrystals (NCs) are promising optoelectronic and catalytic materials. Manipulating their morphology can improve their properties and stability. In this work, an alkene-derived zwitterionic ligand was used to control the morphology of $CsPbBr_3$ NCs to yield the highly unusual rhombicuboctahedron morphology, showcasing the first example of a surfactant-tail controlled growth.

Colloidal $CsPbX_3$ perovskite nanocrystals (NCs) have been used as first-hand chemical templates to the expedite construction of new promising optoelectronic materials, like light emitting diodes (LEDs),[1] lasers,[2] and photodetectors.[3] Traditionally, $CsPbX_3$ NCs are synthetized in a lab scale fashion by hot injection (HI) approaches, using a combination of the respective metal oleates (Cs- and Pb- oleates), oleyl amine/oleic acid (OAm/OA) as capping ligands, and halide sources. To stabilize the NCs' ionic surface, long chain surfactant ligands like OAm (oleyl amine) and OA (oleic acid) are usually employed. However, due to its ionic nature, these ligands can suffer side neutralization reactions mainly when the isolation and purification processes are carried out, promoting a rapid ligand desorption effect.[4] Consequently, the NC system experiences a surface colloidal instability leading to a decrease of photoluminescence quantum yields (PLQYs). To alleviate this, several different approaches have been used, such as the manipulation of the ligand equilibrium with a ligand excess (OA/OAm) to prevent the ligand desorption in the isolation process,[5] and the use of low polarity antisolvents (*i.e.*, methyl acetate) to remove unreacted precursors.[6] More recently, Kovalenko's research group reported the first colloidal $CsPbBr_3$ NCs capped with zwitterionic ligands that were used as surface stabilization agents (lecithin,[7] sulfobetaines,[5] phosphocholines[5] and γ-aminoacids[8]). Among these zwitterionic ligands, they found that cubic $CsPbBr_3$ NCs capped with 3-(*N*,*N*-dimethyloctadecylammonio)-propanesulfonate (ASC18) sulfobetaine exhibited the best colloidal NC surface stability, which leads to an easy material isolation. This effect is a consequence of a chelate effect achieved for the respective ammonium cation and deprotonated acid of the ligand in the NC surface (Fig. 1A). Moreover, it is known that $CsPbBr_3$ NCs capped with both OAm/OA and the zwitterionic ASC18 ligand retain NC cubic shapes.

New concepts

Lead-halide perovskite nanocrystals (NCs), particularly $CsPbBr_3$ NCs, hold immense potential for quantum, optical, and energy applications. Achieving precise control over their morphology and facet growth has been a long-standing challenge. In this study, we introduce a novel approach using alkene-derived zwitterionic ligands to modulate the shape of $CsPbBr_3$ NCs while preserving their high photoluminescence quantum yield. Unlike previous methods that focused on altering the ionic head of surfactants, our novel technique capitalizes on the untapped potential of the ligand's tail-end. Leveraging alkene π–π interactions, we achieve controlled growth, resulting in $CsPbBr_3$ NCs with rare rhombicuboctahedral shapes. This marks the first instance where the ligand tail plays a pivotal role in achieving precise control over specific nanocrystal cubic facets. Beyond morphology control, our findings have far-reaching implications, offering new avenues for designing and manipulating nanocrystals with tailored properties. The vast chemical space provided by the ligand's tail-end offers unprecedented flexibility for tuning the shape and characteristics of these materials, potentially facilitating the development of perovskite nanocrystal superlattices or access to uncommon morphologies. This work advances our understanding of nanocrystal growth and expands the horizons of nanocrystal engineering, opening fresh perspectives and opportunities for innovation in the field.

[a] *Laboratorio de Fisicoquímica y Reactividad de Superficies (LaFReS), Instituto de Investigaciones en Materiales, Universidad Nacional Autónoma de México, Circuito Exterior s/n, CU, Coyoacán, 04510, Ciudad de México, Mexico. E-mail: diego.solis@unam.mx*

[b] *Instituto de Física, Universidad Nacional Autónoma de México, CU, Coyoacán, 04510 Ciudad de México, Mexico*

[c] *Instituto de Investigaciones en Materiales, Universidad Nacional Autónoma de México, CU, Coyoacán, 04510 Ciudad de México, Mexico*

† Electronic supplementary information (ESI) available: Detailed information about materials, methods, and computational details, including the synthetic procedures for the synthesis of ASDC12 and S-ASDC12, their characterization and NMR spectra. Synthetic procedure for the synthesis of $CsPbBr_3$ NCs. TEM micrographs and their respective histograms, and computational details (PDF). See DOI: https://doi.org/10.1039/d3nh00409k

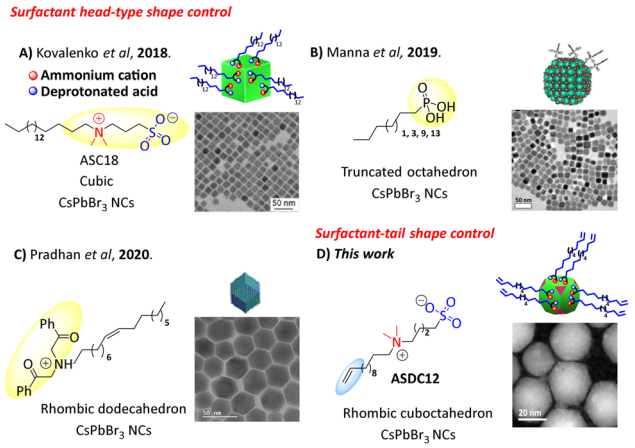

Fig. 1 Schematic representation of literature documented ligands for the synthesis of $CsPbBr_3$ NCs and their respective NC morphologies. (A) Adapted with permission from ref. 8. Copyright 2018 American Chemical Society. (B). Adapted with permission from ref. 9. Copyright 2019 American Chemical Society. (C). Adapted with permission from ref. 10. Copyright 2020 American Chemical Society. (D) Our work, surfactant-tail control of $CsPbBr_3$ NCs morphology.

While most perovskite nanocrystals (NCs) exhibit a cubic morphology, recent studies have demonstrated the ability to fine-tune the intrinsic optical and catalytic properties of lead bromide perovskite NCs by precisely controlling facet growth and shape.[11] In this vein, synthetic efforts to modulate the shape of $CsPbBr_3$ NCs have been extensively carried out, either by the addition of other metals like Cd and Mn,[12] by lowering the injection temperature, by post synthetic modifications of Cs_4PbBr_6 NCs,[13] or by changing the commonly used long-chain ligands to short-chain amines.[14] However, few reports focus on studying the effect of other surfactants than OAm/OA as capping ligands in the facet growth of $CsPbBr_3$ NCs. Some of these examples include the Manna group's synthesis of highly stabilized colloidal $CsPbBr_3$ NCs with truncated octahedron morphology by passivating the NC surface with alkyl-phosphonic acids as capping ligands (Fig. 1B). The phosphonate ligands showed a large affinity for the NC surface, stabilizing the {001} and {110} NC facets.[9] Also, rhombic dodecahedron-shaped $CsPbBr_3$ NCs were reported by Pradhan *et al.* using α-bromoketone as a capping ligand.[10] The resultant quasi-spherical particles were stabilized by tertiary ammonium ions synthesized by consecutive S_N2 reactions of the corresponding bromoketone with OAm. These tertiary cations passivated the {200}, {020}, and {112} $CsPbBr_3$ NC facets (Fig. 1C). Notably, all these approaches use the ligand "head-part" to control the nanocrystal morphology evolution. To the best of our knowledge, this is the first report in which the use of a terminal functional group of the capping ligand is able to modulate the nanocrystal facet growth. This is beneficial as it would allow the retention of the functional properties that some of these "heads" have, such as phosphonic acids, or zwitterionic ligands. Furthermore, while there are a limited number of "heads" that can beneficially interact with the NC surface, there is potentially an infinite number of "tails" that can be explored and exploited. Herein, we propose the use of a ligand with a terminal functional group, which can act as a remote control for the $CsPbBr_3$ NC facet growth. Specifically, our ligand, a zwitterionic ligand, combines a head group that can stabilize efficiently the nanocrystal surface (sulfobetaine), and a terminal double bond which can promote a homogeneous ligand ordering on the nanocrystal surface. Remarkably, the introduction of the alkene moiety in the surfactant tail resulted in $CsPbBr_3$ NCs with a rare rhombicuboctahedron (SRO) shape (Fig. 1D). We synthesized our capping ligand, ASDC12 (4-(dodec-11-en-1-yldimethylammonio)butane-1-sulfonate), through a sequential halide elimination (E_2) and S_N2 type reactions starting from 1,12-dibromododecane (see the ESI,† for complete synthetic details). Importantly, ASDC12 can be obtained in three steps with good yields (49% after 3 steps).

In an initial experiment, we carried out the colloidal $CsPbBr_3$ NC synthesis using ASDC12 as a ligand through a hot-injection procedure adapted from the original report by Krieg and collaborators (see the ESI,† for details).[15] Additionally, the synthesis of $CsPbBr_3$ NCs capped with the typical OAm and OA ligands was carried out following the same modified procedure and used as a control experiment. To confirm the overall structure of the synthesized NCs, powder X-ray diffraction (PXRD) was carried out (Fig. 2B) and compared to the patterns of the OA/OAm NCs and $CsPbBr_3$ bulk material. Both diffraction patterns matched the orthorhombic phase of $CsPbBr_3$ (PDF 01-072-7929). It is noted that the ASDC12-protected and OA/OAm-protected NCs presented similar diffraction patterns obeying their nanoscale size. Fig. 2C shows a low-magnification TEM image, which reveals the size and shape distribution of the ASDC12-protected NCs. The average length of the particles was 27.1 ± 4.1 nm (aspect ratio = 1.1). $CsPbBr_3$ NCs commonly crystallize in a cubic shape when zwitterionic ligands are used in their synthesis; however, a prominent truncation from the cubic shape is evident when using ASDC12. When describing nanoparticle faceting, the

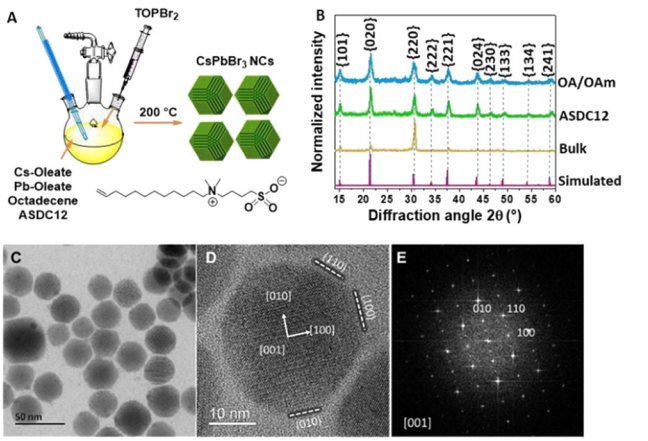

Fig. 2 Synthesis of $CsPbBr_3$ NCs capped with ASDC12: (A) schematic representation of our synthetic approach. (B) PXRD patterns of $CsPbBr_3$ synthesized by HI and in bulk form. (C) Typical transmission electron microscopy (TEM) images of truncated cube $CsPbBr_3$ NCs, and (D) HRTEM micrographs of $CsPbBr_3$ NCs. (E) FFT image of truncated $CsPbBr_3$ NCs.

cubic structure nomenclature is more commonly used since it is easily visualized; *i.e.*, the $\{001\}_{ort}$, $\{110\}_{ort}$, $\{0\underline{1}0\}_{ort}$, and $\{112\}_{ort}$, can be described as the $\{001\}_{cub}$, $\{010\}_{cub}$, $\{100\}_{cub}$, and $\{011\}_{cub}$, respectively. For convenience and easiness, the cubic nomenclature shall be used during this manuscript to describe the particle facets. Fig. 2D and E correspond to a high-magnification HRTEM image of a single NC and its corresponding fast Fourier transform (FFT), which highlights the crystal symmetry. The particle is oriented along the [100] zone axis (cubic nomenclature), a common direction when imaging nanocubes because of their {100} enclosed shape, laying in an ordered manner on the carbon support. In our case, the {011} truncation is evident, modifying the external shape of the particles. The truncation of a cube can lead to different morphologies with different exposed facets, such as truncated cubes, truncated octahedrons, cuboctahedrons, rhombic dodecahedrons, *etc.* The resultant shape will depend on the truncation plane and faceting degree.[16] The shape determination of the synthesized NCs was performed by analyzing intensities from high-angle annular dark-field (HAADF) images of individual NCs, since the projected contrast depends on the sample thickness (mass-thickness contrast). Intensity profiles were acquired across the particle center and edges and compared to ideal thickness projections of different NC shapes (Fig. 3). Particles oriented along two orientations were compared: the [100] direction, in which the projected shape forms an octagonal contour (Fig. 3A), and the [111] direction, which is seen as a hexagonal shape (Fig. 3C). The acquired profiles were compared to the ideal thickness projection of different polyhedrons. The analysis showed a good correlation with a small rhombicuboctahedron (SRO), whose thickness profile is superimposed on the plots (Fig. 3B and D). The SRO can be viewed as a doubly-truncated octahedron with enlarged {110} facets, sketched in Fig. 3E. The SRO consists of twelve {011}, eight {111}, and six {100} external facets, differing from other truncated shapes by the extension of their facets, and only a few groups have reported the SRO shape.[9,17] The obtained SRO shape highlights the capabilities of the ASDC12 ligand to stabilize crystal planes other than the {100} facets present in most $CsPbX_3$ NCs.

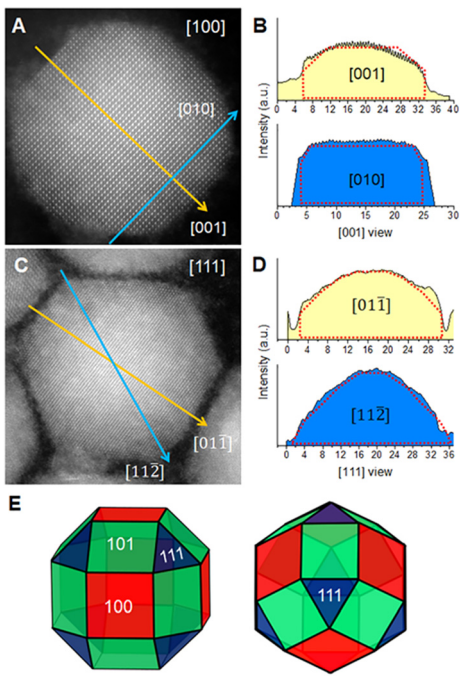

Fig. 3 (A) and (C) HAADF images of single ASDC12-capped NCs oriented along the [100] and [111] zone axes, respectively. (B) and (D) Intensity line profiles along the indicated directions for shape determination. Red dotted-lines correspond to the ideal thickness profiles of a rhombicuboctahedron along the indicated directions. (E) Sketches of the rhombicuboctahedron.

In order to explore the ligand concentration effect in the NC synthesis, we carried out the synthesis using 0.25 mmol, 0.375 mmol, and 1.0 mmol of ASDC12 while keeping the concentration of the remaining precursors constant. As shown in Fig. 4A, well-defined cubic $CsPbBr_3$ NCs with an average length of 17.3 nm were obtained when adding 0.25 mmol of ASDC12. However, when adding 0.375 mmol or 1.0 mmol of ASDC12, the formation of truncated $CsPbBr_3$ NCs was promoted, although in a minor proportion compared to the SRO synthesis (Fig. 4B and D). Moreover, the average size increased from 22.1 nm to 32.2 nm when increasing the ligand concentration (Fig. 4B–D). The ligand concentration can also modify the NC's aspect ratio. When using 0.375 mmol, the aspect ratio increased to 1.3, leading to rectangular nanoprisms with a slight truncation (Fig. 4B). We note that the average size of the nanocrystals increases with increasing ligand concentration for ligand ASDC12. Both behaviors have been reported in the literature.[18] To provide a quantitative perspective on the truncated shape of the produced particles, we calculated the truncation degree index, τ, using the method outlined by Disch and coworkers[19] (see the ESI,† for details). Herein, a τ value of 0 represents a perfect cubic shape, whereas a value nearing 1 indicates a significantly truncated form. When increasing the ASDC12 concentration to 0.25, 0.375, 0.5 and 1 mmol, τ was 0.30, 0.26, 0.72, and 0.33, respectively, as observed in Fig. 4A–D. It can be noted how the correct ligand concentration led to the formation of the highly-truncated SRO shape.

While zwitterionic ligands (and many other ligands) commonly generate $CsPbBr_3$ NCs with a cubical shape, herein, the presence of a terminal double bound in the tail of our ligand allows the shape modulation of the NCs. Even though more studies are needed, our current hypothesis is that the double bond allows an enhancement of the ligand packing by alkene π–π interactions, which subsequently leads to the truncation of the cubic shape.[20] In fact, similar behavior has been observed in the formation of anisotropic NCs.[21] To support this hypothesis we experimentally determined the ligand density of ASDC12 and S-ASDC12 molecules on the surface of the NCs through quantitative nuclear magnetic resonance (qNMR, see experimental details in the ESI†).[22,23] Notably, we found a ligand density of 4.9 ligand per nm^2 for ASDC12, which is significantly higher than the S-ASCD12 value (2.6 ligand per nm^2), and other values reported in the literature[8,24] that range from 1.2 to 2.8 ligand per nm^2.

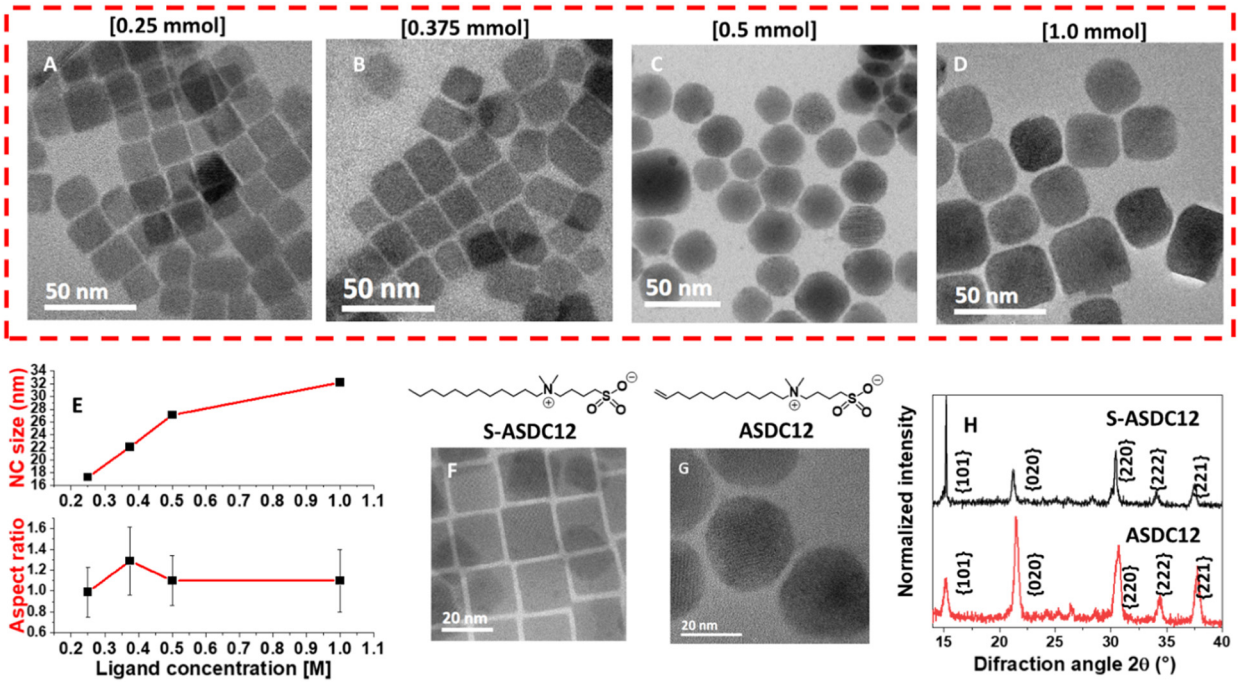

Fig. 4 (A)–(D) TEM analysis of $CsPbBr_3$ NCs synthesized at different ASDC12 concentrations; (E) changes in the size and NC ratio of $CsPbBr_3$ NCs at different ASDC12 concentrations; (F) and (G) Chemical structure of S-ASDC12 and ASDC12 and TEM images of their respective NCs (G). (H) PXRD patterns of NCs capped with S-ASDC12 (gray) and ASDC12 (red).

To further demonstrate that the terminal double bound in ASDC12 is pivotal to promoting truncation of the perovskite NCs, a saturated version of the zwitterionic ligand (S-ASDC12) was synthesized and used instead of ASDC12 as a control experiment (see the ESI,† for detailed methods). When the NCs' synthesis was performed in the presence of S-ASDC12, $CsPbBr_3$ perovskite {100} enclosed nanocubes were obtained, similarly to OA/OAm-protected NCs (Fig. 4F). The produced cubic NCs had a smaller average length (12.0 ± 1.5 nm) compared with the ASDC12-protected SRO (27.1 ± 4.1 nm), but the facet affinity changed entirely by the presence of the double bond in the ASDC12 ligand, which was retained after carrying out our hot injection protocol (see Fig. S6 in the ESI†), having a competing stabilization effect of the {100}, {011}, and {111} facets forming the SRO morphology. Ligand concentration studies in $CsPbBr_3$ NCs capped with S-ASDC12 showed that the particle size increased inversely with the concentration of S-ASCD12, being 23.5 nm, 12.0 nm, 33.9 nm, and 39.9 nm for 1 mmol, 0.5 mmol, 0.375 mmol, and 0.25 mmol, respectively. The calculated τ values for these samples were 0.30, 0.24, 0.25, and 0.34, respectively (see Fig. S13 in the ESI†). It is seen that although truncation was also observed with the S-ASDC12 ligand, the truncation degree was favored for the ASCD12 ligand at the precise concentration of 0.5 mmol, exposing {011}, {111}, and {100} facets, with a much better control over the size and shape distribution compared to the saturated ligand.

The $CsPbBr_3$ perovskite phase was corroborated by PXRD analysis (Fig. 4H), in which the difference in peak intensity between both samples reflects the crystallographic texture that results from the preferential [100] accommodation of cubic NCs on the substrate compared to a more rounded SRO shape being able to lay in a different orientation. To gain a deeper understanding of the influence of different ligands, specifically the role of the double bond, on the final shape of the nanocrystals (NCs), we employed density functional theory (DFT) calculations. Our focus was on studying the differences in interactions between unsaturated and saturated hydrocarbon chains. As proxies for ASDC12 and S-ASDC12, we selected 1-dodecene and dodecane, respectively, and added 6-dodecene to compare the role of the double bond in the middle of the hydrocarbon chain. Using these three molecules, we created a grid of nine molecules to investigate their packing and interactions (see the ESI,† for a complete description). Upon optimization, our calculations revealed two main findings. Firstly, the unsaturated chain representing ASDC12 exhibited significantly closer packing, with interchain C–C distances ranging from 3.72 to 4.09 Å, compared to 3.90 to 4.10 Å for S-ASDC12. This discrepancy in distances can be attributed to the interaction between the unsaturated (sp^2) carbons of dodecene.

Notably, we found a C_{sp^2}–C_{sp^2} distance of 3.72 Å, which lies in the expected range for alkene π–π interactions. Furthermore, by comparing the two arrays, we were able to estimate that the difference in interaction between them is 1.6 kcal mol^{-1}. Significantly, our findings reveal that the interaction energy in 1-dodecene also surpasses that in 6-dodecane by 4.4 kcal mol^{-1}, underscoring the critical role of tail-end interactions over those in the middle. Importantly, the interaction energy found for

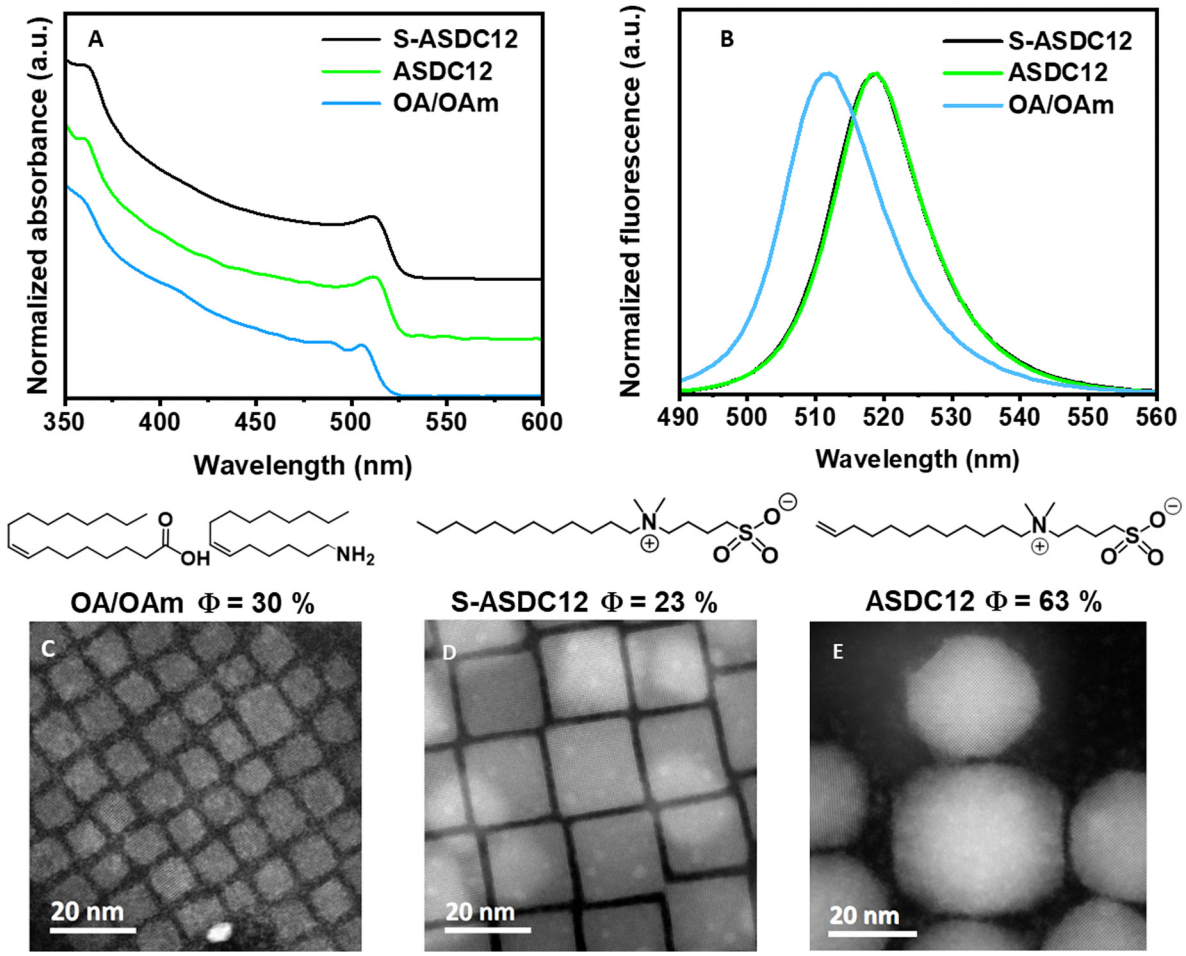

Fig. 5 Absorbance (A) and PL (B) spectra of $CsPbBr_3$ NCs capped with OA/OAm, and (C)–(E) HAADFpn images and their respective PLQY (Φ).

1-dodecene is consistent with previously reported values for alkene–alkene dimers.[25] These results confirm the significant impact of the double bond in terms of both packing and energetics, both of which ultimately result in improved binding to the NC surface.[26] Another possible explanation is the interaction between the solvent used in the synthesis (octadecacene) and the double bond of ASDC12. Herein, a similar alkene-alkene interaction would be responsible for the observed differences.[26] While we acknowledge that the density of ligands on the surface of NCs is likely to be considerably lower and that the energetic difference is relatively small compared to other competing processes, it is essential to note that all other factors remained exactly equal, including the reaction conditions, concentration, and temperature. Thus, we attribute the observed differences in the final product to these interactions and the role that they play during the NC growth.

Once the structural characterization of the respective $CsPbBr_3$ NCs was obtained, we conducted their optical characterization. The $CsPbBr_3$ NCs capped with S-ASDC12 and ASDC12 showed a photoluminescence (PL) emission at 518 nm and 519 nm, respectively, whereas the OA/OAm-capped NCs exhibited a 6 nm blue-shift with a maximum peak at 511 nm (Fig. 5A). These results are expected due to quantum confinement effects according to their respective size.[27] Following on from this, the ASDC12 and S-ASDC12-capped NCs PL emission showed a full width at half maximum (FWHM) of 15.5 nm and 15.4 nm (Fig. 5B), respectively, while the OA/OAm-capped $CsPbBr_3$ NCs showed a wider emission with an FWHM of 19.2 nm, even though these nanocrystals showed a narrower size distribution compared with the nanocrystals capped with the zwitterionic ligands ASDC12 and S-ASDC12 (see the ESI,† for complete details). All $CsPbBr_3$ nanocrystals have a small green FWHM fluorescence emission value, which denoted higher nanocrystal uniformity. Furthermore, the respective PLQY $CsPbBr_3$ capped with ASDC12 is Φ = 63%, higher than the PLQY's obtained for the NCs capped with OA/OAm and S-ASDC12 (30% and 23%, respectively). These results are somewhat expected because the $CsPbBr_3$ NCs capped with ASDC12 presented a better ligand packing in the nanocrystal surface due to the π–π interactions in the terminal alkene moiety, which promotes a better colloidal stabilization and passivation together with the increase of the PLQY (Fig. 5C–E).

Conclusions

In conclusion, we have successfully synthesized $CsPbBr_3$ perovskite nanocrystals capped with an alkene-derived zwitterionic

ligand that can remotely control the growth of {111} cubic facets, resulting in the rare rhombicuboctahedron shape. Our TEM and HRTEM analyses demonstrate that the use of ASDC12 as a capping ligand stabilizes crystal planes other than the {100} facets present in the commonly obtained $CsPbBr_3$ NCs. Importantly, we demonstrated that not only the head moiety of the capping ligand can modulate the NC morphology, but also the tail-end can have drastic effects, while retaining some of the advantages of a given head group. In this particular case, the modulation probably occurs *via* alkene π–π interactions, which enhance the ligand packing around the $CsPbBr_3$ nanocrystal surface. This approach provides a promising alternative route for fine-tuning the shape and properties of perovskite nanocrystals, and for directing the formation of perovskite NC superlattices. In our future work, we plan to further explore this strategy and leverage the tools of organic chemistry to fully exploit the concept of surfactant-tail control.

Author contributions

Y. A. A.-S. was responsible for the research project and carried out the ligand organic synthesis, processed all data for material characterization and obtained the $CsPbBr_3$ NCs; B. V. obtained the first $CsPbBr_3$ NC conditions, processed PXRD measurements and obtained $CsPbBr_3$ at different ligand concentrations; J. E. R.-I. obtained the $CsPbBr_3$ NC TEM images; R. M.-C. funded, analysed and processed TEM data; E. R. carried out the computational analysis; D. S.-I. was responsible for the conceptualization, supervision, analysis, manuscript writing and funding acquisition. Y. A. A.-S., B. V., R. M.-C. and D. S.-I. wrote the paper.

Conflicts of interest

There are no conflicts to declare.

Acknowledgements

We thank CONACYT CB-A1-S-8729 for support of this work. Y. A. A.-S. acknowledges the support from DGAPA-UNAM postdoctoral fellowship. We are grateful to Prof. A. Paulina Gómora-Figueroa for granting us access to several instruments. R. M.-C. acknowledges DGAPA-PAPIIT grant IA-106623. E. R. acknowledges DGAPA-PAPIIT grant IG100320 and LANDCAD-UNAM-DGTIC-225. Finally, we acknowledge the support from Adriana Tejeda, Gerardo Cedillo, Carlos Ramos, Alejandro Pompa, and Miguel Angel Canseco.

References

1 Y. H. Kim, S. Kim, A. Kakekhani, J. Park, J. Park, Y. H. Lee, H. Xu, S. Nagane, R. B. Wexler, D. H. Kim, S. H. Jo, L. Martínez-Sarti, P. Tan, A. Sadhanala, G. S. Park, Y. W. Kim, B. Hu, H. J. Bolink, S. Yoo, R. H. Friend, A. M. Rappe and T. W. Lee, *Nat. Photonics*, 2021, **15**(2), 148.
2 Q. Zhang, Q. Shang, R. Su, T. T. H. Do and Q. Xiong, *Nano Lett.*, 2021, **21**(5), 1903.
3 T. Yang, F. Li and R. Zheng, *ACS App. Electron. Mater.*, 2019, **1**(8), 1348.
4 S. Mourdikoudis, M. Menelaou, N. Fiuza-Maneiro, G. Zheng, S. Wei, J. Pérez-Juste, L. Polavarapu and Z. Sofer, *Nanoscale Horiz.*, 2022, **7**, 941.
5 R. Grisorio, M. E. Di Clemente, E. Fanizza, I. Allegretta, D. Altamura, M. Striccoli, R. Terzano, C. Giannini, M. Irimia-Vladu and G. P. Suranna, *Nanoscale*, 2019, **11**(3), 986.
6 A. Swarnkar, A. R. Marshall, E. M. Sanehira, B. D. Chernomordik, D. T. Moore, J. A. Christians, T. Chakrabarti and J. M. Luther, *Science*, 2016, **354**(6308), 92.
7 F. Krieg, Q. K. Ong, M. Burian, G. Rainò, D. Naumenko, H. Amenitsch, A. Süess, M. J. Grotevent, F. Krumeich, M. I. Bodnarchuk, I. Shorubalko, F. Stellacci and M. V. Kovalenko, *J. Am. Chem. Soc.*, 2019, **141**(50), 19839.
8 F. Krieg, S. T. Ochsenbein, S. Yakunin, S. Ten Brinck, P. Aellen, A. Süess, B. Clerc, D. Guggisberg, O. Nazarenko, Y. Shynkarenko, S. Kumar, C. J. Shih, I. Infante and M. V. Kovalenko, *ACS Energy Lett.*, 2018, **3**(3), 641.
9 B. Zhang, L. Goldoni, J. Zito, Z. Dang, G. Almeida, F. Zaccaria, J. De Wit, I. Infante, L. De Trizio and L. Manna, *Chem. Mater.*, 2019, **31**(21), 9140.
10 S. Bera, R. K. Behera and N. Pradhan, *J. Am. Chem. Soc.*, 2020, **142**(49), 20865.
11 N. Pradhan, *ACS Energy Lett.*, 2021, **6**(1), 92.
12 S. Bera, A. Patra, S. Shyamal, D. Nasipuri and N. Pradhan, *ACS Energy Lett.*, 2022, **7**(9), 3015.
13 J. Wu, S. Zhao, X. Chi, N. Sui, Z. Kang, Q. Zhou, H. Zhang, X. Li, B. Zhao and Y. Wang, *J. Phys. Chem. C*, 2021, **125**(45), 25044.
14 A. Pan, B. He, X. Fan, Z. Liu, J. J. Urban, A. P. Alivisatos, L. He and Y. Liu, *ACS Nano*, 2016, **10**(8), 7943.
15 F. Krieg, S. T. Ochsenbein, S. Yakunin, S. ten Brinck, P. Aellen, A. Süess, B. Clerc, D. Guggisberg, O. Nazarenko, Y. Shynkarenko, S. Kumar, C. J. Shih, I. Infante and M. Kovalenko, *ACS Energy Lett.*, 2018, **3**(3), 641.
16 A. S. Barnard, *Nanotechnology*, 2013, **24**(8), 085703.
17 Q. A. Akkerman, T. P. T. Nguyen, S. C. Boehme, F. Montanarella, D. N. Dirin, P. Wechsler, F. Beiglböck, G. Rainò, R. Erni, C. Katan, J. Even and M. Kovalenko, *Science*, 2022, **377**(6613), 1406.
18 (*a*) S. K. Dutta, L. Peng, B. Hudait, R. Xie and N. Pradhan, *ACS Energy Lett.*, 2022, **7**(9), 3177; (*b*) F. Haydous, J. M. Gardner and U. B. Cappel, *J. Mater. Chem. A*, 2021, **9**, 23419; (*c*) N. Pradhan, D. Reifsnyder, R. Xie, J. Aldana and X. Peng, *J. Am. Chem. Soc.*, 2007, **129**, 9500; (*d*) S. Mozaffari, W. Li, M. Dixit, S. Seifert, B. Lee, L. Kovarik, G. Mpourmpakis and A. M. Karim, *Nanoscale Adv.*, 2019, **1**, 4052.
19 S. Disch, E. Wetterskog, R. P. Hermann, G. Salazar-Alvarez, P. Busch, T. Brückel, L. Bergström and S. Kamali, *Nano Lett.*, 2011, **11**, 1651.
20 (*a*) H. Heinz, C. Pramanik, O. Heinz, Y. Ding, R. K. Mishra, D. Marchon, R. J. Flatt, I. Estrela-Lopis, J. Llop, S. Moya and

R. F. Ziolo, *Surf. Sci. Rep.*, 2017, **72**(1), 1; (*b*) T. Chen, M. Li and J. Liu, *Cryst. Growth Des.*, 2018, **18**(5), 2765.

21 L. Bazán-Díaz, R. Mendoza-Cruz, J. J. Velázquez-Salazar, G. Plascencia-Villa, D. Romeu, J. Reyes-Gasga, R. Herrera-Becerra, M. José-Yacamán and G. Guisbiers, *Nanoscale*, 2015, **7**(48), 20734.

22 C. Pareja-Rivera, A. L. Solís-Cambero, M. Sánchez-Torres, E. Lima and D. Solis-Ibarra, *ACS Energy Lett.*, 2018, **3**(10), 2366–2367.

23 Y. Chen, S. R. Smock, A. H. Flintgruber, F. A. Perras, R. L. Brutchey and A. J. Rossini, *J. Am. Chem. Soc.*, 2017, **142**, 6117–6127.

24 (*a*) S. R. Smock, T. J. Williams and R. L. Brutchey, *Angew. Chem., Int. Ed.*, 2018, **57**, 11711–11715; (*b*) R. Grisorio, F. Fasulo, A. B. Muñoz-García, M. Pavone, D. Conelli, E. Fanizza, M. Striccoli, I. Allegretta, R. Terzano, N. Margiotta, P. Vivo and G. P. Suranna, *NanoLett.*, 2022, **22**, 4437–4444; (*c*) M. Imran, P. Ijaz, L. Goldoni, D. Maggioni, U. Petralanda, M. Prato, G. Almeida, I. Infante and L. Manna, *ACS Energy Lett.*, 2019, **4**, 819–824.

25 J. R. Premkumar, D. Umadevi and G. N. Sastry, *Indian J. Chem.*, 2014, **53**, 985–991.

26 J. Zito and I. Infante, *Acc. Chem. Res.*, 2021, **54**(7), 1555.

27 (*a*) Y. Bekenstein, B. A. Koscher, S. W. Eaton, P. Yang and A. P. Alivisatos, *J. Am. Chem. Soc.*, 2015, **137**(51), 16008; (*b*) Y. Dong, T. Qiao, D. Kim, D. Parobek, D. Rossi and D. H. Son, *Nano Lett.*, 2018, **18**, 3716–3722.

